Chapter One

Introduction

The phenomenon variously known as the corona wind, electric wind or ionic wind was first reported by Francis Hauksbee, curator of instruments for the Royal Society of London, in 1709. Holding a charged tube close to his face, he wrote,

> "... the Force of the [electrical] Effluvia was render'd manifest to ... [the] Sense ... of feeling. They ... were plainly to be felt upon the Face ... if the rubb'd tube were held near it. An they seemed to make very nearly such sort of stroaks upon the Skin as a number of fine limber Hairs pushing against it..."
> (Robinson, 1962)

Yet, despite the enormous growth of interest in the study of electricity and electrical-related phenomena from the 1800s and the attention of such notaries as Newton, Faraday and Maxwell, the corona wind remained essentially as a curio to be used at science fairs, until the last twenty years. Literature on the corona wind prior to the 1970s is scarce, and its potential applications were limited by the technology of the day. On the other hand, corona discharges have found applications in many fields of industry.

Corona discharges are generated when a high potential is applied to electrodes in a non-uniform field configuration, such as a point to plane. The ionisation region around the point creates ions of the same polarity as the point, which move out into the discharge gap. Thus, corona discharges are often used as a source of ions in equipment ranging from large-scale industrial electrostatic precipitators to the office photocopier and laser printer. However, unwanted corona discharges within high-voltage gas insulation systems cause enormous problems for the power industry through power losses and equipment damage.

The ions produced by the corona discharge moving under the influence of the electric field collide with neutral gas molecules and transfer momentum to these neutrals. Thus, there is a bulk movement of the neutral gas associated with a corona discharge and this is the corona wind. Despite the presence of a corona wind whenever a corona discharge occurs, the corona wind was largely ignored until the 1970s when it was found that establishing a corona discharge above a heated surface enhanced the transfer of heat and mass from that surface. This phenomenon was found to be due to the action of the corona wind and interest grew in the processes involved in the production of the corona wind.

The corona wind can be observed by flow visualisation techniques, and its effects can be judged by determining the pressure due to the wind at some distance from the discharge. Yet, to date, there has been no satisfactory technique to measure the speed of the corona wind within the discharge gap. Techniques which have been used to measure the speed of the wind have employed conventional flow measuring systems, such as hot-wire anemometers and laser Doppler anemometry. However, with a hot-wire anemometer a conducting surface must be introduced into the discharge gap, causing field distortions and drawing current from the discharge. Laser Doppler anemometry, on the other hand, measures the speed of charged particles introduced into the discharge and these move under the combined influence of the corona wind and the electric field, causing overestimation of the speed of the corona wind.

In order to gain a complete understanding of the corona wind, accurate measurements of the speed of the wind are required. With the advent of the optical fibre as a waveguide for the communications industry in the 1970s, much work on the physical properties of the optical fibre was performed. As a result, optical fibres have been applied to the sensing of a wide range of physical and chemical parameters. Probing electrical discharges with optical fibre sensors has several advantages over more conventional techniques; optical fibres are dielectrics, which cause none of the field disturbances and breakdown problems associated with metal probes, their small dimensions means

that field distortion is minimised and signal transfer and processing are possible in electromagnetically-noisy environments. Thus, optical fibre sensing provides a technique for the measurement of corona wind speeds which does not disturb the mechanism producing it, that is, the corona discharge.

In this thesis, the speed of the corona wind is measured in both an atmospheric air corona and, for the first time, in a sulphur hexafluoride (SF_6) corona discharge. Two optical techniques are used in atmospheric air; laser Doppler anemometry and optical fibre sensing. The first technique is a conventional technique for measuring flow speeds and therefore acts as a check for the new technique of optical fibre sensing. Optical fibre sensing provides an unambiguous corona wind speed measurement within the discharge gap and, when compared to the results obtained by laser Doppler anemometry, provides useful information about the movement of charged particles within the discharge.

Within the electrical power industry, high-pressure SF_6 gas is used to insulate high voltage systems. Within these systems corona discharges may occur at any sharp edges and points. A corona discharge dissociates the SF_6 and such insidious corona discharges can ultimately lead to failure of the system. Whenever a corona discharge is established the corona wind is generated, but the corona wind in SF_6 has, up to now, not been investigated. The work presented in this thesis is the first to provide measured corona wind-speed profiles for an SF_6 corona discharge.

Chapter 2 of the thesis is a literature review of our present understanding of the corona wind and methods which have been used, to date, to measure it. Further, corona discharges in air and SF_6 are discussed, as are applications of corona discharges and the corona wind. In Chapter 3, a review of optical fibre sensing is presented. The experimental arrangements for both optical fibre sensing and laser Doppler anemometry are described in Chapter 4. The results of the optical fibre sensing and the laser Doppler anemometry measurements of the corona wind in atmospheric air are presented in Chapter 5, along with a comparison of the two measurement techniques. Chapter 6 presents the first ever three-dimensional measurements of the corona wind in an SF_6 corona discharge, along with a comparison between the results obtained in air and SF_6.

Chapter 7 deals with two separate topics, which arose from the experimental study of the corona wind with an optical fibre. Firstly, because the optical fibre sensor required heating of the fibre the response of the fibre to high temperatures was examined. Secondly, because streamers associated with the onset of the corona discharge were found to disrupt the sensor, this effect is discussed. Finally, Chapter 8 presents a summary and general conclusions.

Chapter 2

Corona Discharges and the Corona Wind

The properties of the corona wind are directly related to the corona discharge itself. Therefore, an understanding of the corona wind must be preceded by an understanding of the corona discharge. In Sections 2.1 and 2.2 of this chapter corona discharges in air and sulphur hexafluoride (SF_6) are reviewed, with emphasis on the positive dc corona discharge in a point-plane electrode configuration. A few of the many, varied uses of corona discharges are briefly discussed in Section 2.3. Having established a basis for the discussion, Section 2.4 details the production mechanism of the corona wind and a theoretical treatment of the corona wind is presented in terms of electrohydrodynamic (EHD) theory.

The corona wind generates interest in areas such as heat and mass transfer applications, and in areas of application of corona discharges. The role of the corona wind in devices which use corona discharges is not fully understood and this is particularly true in electrostatic precipitators and in high-voltage SF_6-insulated systems. All of these areas of interest are discussed in Section 2.5. Finally, since some data on corona wind speed presented in later chapters of the thesis were obtained using laser Doppler anemometry (LDA), details of this technique, and measurement techniques used by other researchers to study the corona wind, are examined in Section 2.6.

2.1 Corona discharges in air

A corona discharge occurs when a high potential is applied between electrodes in a non-uniform field geometry. Geometries which are commonly used to produce non-uniform electric fields are point-plane (also called rod-plane); wire-plane; and coaxial cylinders (wire-cylinder). In these geometries the stressed electrode would be the point (rod) and the wire, respectively. As the Laplacian electric field is increased at the stressed electrode, a region of gas ionisation is produced in a confined volume close to the high voltage electrode. The electric field over most of the discharge gap is too low for breakdown of the entire gap, even when the electrode potential is at arc threshold. The free charges created in the high-field region move out into the low-field drift region where no further ionisation takes place. Therefore, most of the corona gap is filled with ions of the same polarity as the point, moving away from the point electrode. It is the presence of this low-field drift region in corona discharges which prevents arcing across the gap. The passive electrode is characterised by a low electric field and acts mainly as a collecting electrode.

The spatial and temporal details of a corona discharge depend on the polarity of the stressed electrode, the electrode separation, the pressure and type of gas and the actual electrode geometry (Sigmond and Goldman, 1983). Other factors which can effect the nature of the discharge are the presence of a dielectric barrier near the discharge (Abdel-Salam *et al.*, 1997b); the impurities present in the gas (Berger and Senouci, 1997); and the condition of the electrode surfaces (MacGregor e*t al.*, 1986).

If the stressed electrode is of negative polarity, it is the positive ions which are attracted to the electrode and the electrons that move into the low-field region. There the electrons attach to any electronegative atoms or molecules that are present, such as those of oxygen or fluorine. Thus, in a negative corona discharge, it is the negative ions which carry most of the current to the plane electrode. In a non electron-attaching gas, such as nitrogen (N_2), it is the electrons which carry the current and the current is higher than that observed in air. A negative corona discharge in an electronegative gas, such as air, may take the form of a glow discharge or it may be pulsed. When the corona discharge is pulsed the pulses are known as Trichel pulses after their discoverer (Trichel, 1938). In air these pulses are regular and the pulse height is of the order of 1 to 2 mA (Cross, 1987).

This thesis deals primarily with the corona wind produced by positive dc corona discharges in point-plane geometry, and so the discussion of corona discharges will focus on this type of corona.

2.1.1 The positive corona discharge in air

When a positive voltage, which is below the corona onset potential, is applied to a point electrode, initially, the electric field is governed by Laplace's equation. This Laplacian electric field confines the ionisation region and the electrons produced from the ionisation process avalanche towards the anode. The positive ions drift into an electric field of decreasing intensity and do not gain sufficient energy for further ionisation to occur or to generate secondary electrons from the collecting electrode. Due to the fundamental stochastic nature of electron multiplication and feedback, as the anode potential approaches the corona onset potential, an avalanche in the ionisation region may die out or it may cause further avalanches. Thus, the corona current near onset is erratic with small current pulses mixed with larger pulses and periods of no current. This regime is known as the 'burst pulse' regime (Sigmond, 1983).

As the anode potential is further increased photons produced in the high-field region give rise to further ionisation in the gas and may cause photoemission of electrons at the cathode. In atmospheric air, the secondary electrons attach to oxygen atoms and molecules in the low-field region and are then detached by photons or via collisional detachment in the high-field region. Thus, secondary electrons are available and this allows a self-sustained discharge to exist. A positive dc self-sustained corona discharge takes the form of a steady glow which is clearly visible in a narrow region around the point anode. Figure 2.1 is an example of a steady glow corona discharge in atmospheric air.

With the creation of a self-sustained discharge, the region close to the anode has a large density of charged particles compared to the remainder of the gap. Thus, there is distortion of the electric field and, due to the repulsion of ions from the anode, the ionisation region close to the anode acts as a source of charged particles. Consequently, Poisson's equation governs the shape of the electric field in a self-sustained steady corona discharge. The simplest corona geometry which can be theoretically analysed is that of a high-voltage wire on the axis of a cylinder. In this case the problem is reduced to one-dimension as the field is radial and independent of the distance z, between the wire and cylinder and angle about the wire. Figure 2.2 shows the electric field in a wire-cylinder corona discharge as a function of distance from the wire, A: prior to onset of the discharge, B: with low space charge and C: with high space charge such as when charged particles are present in the gap (Cross, 1987). Appendix A gives a theoretical solution to Laplace's equation in point-plane geometry when the point is a hyperboloid of revolution, which is one of the electrode configurations

used in this study. Solution of Poisson's equation for this geometry is not trivial and computer models with many simplifying assumptions are usually called for.

In the bulk of the discharge gap the current is carried by the positive ions which are moving away from the point anode. Late last century Warburg (1899) showed experimentally that the current *I,* at the plane of a point-plane geometry, is given by

$$I = I_0 \cos^5 \theta \qquad (2.1)$$

where θ is the angle to the discharge axis and I_0 is the current on the discharge axis.
The current is found to be concentrated around the discharge axis with 97% of the current falling within an angle of 60° of the axis. The current density at the plane of a positive glow corona similar to that used in the present study is shown in Figure 2.3 (Lamb, 1992).

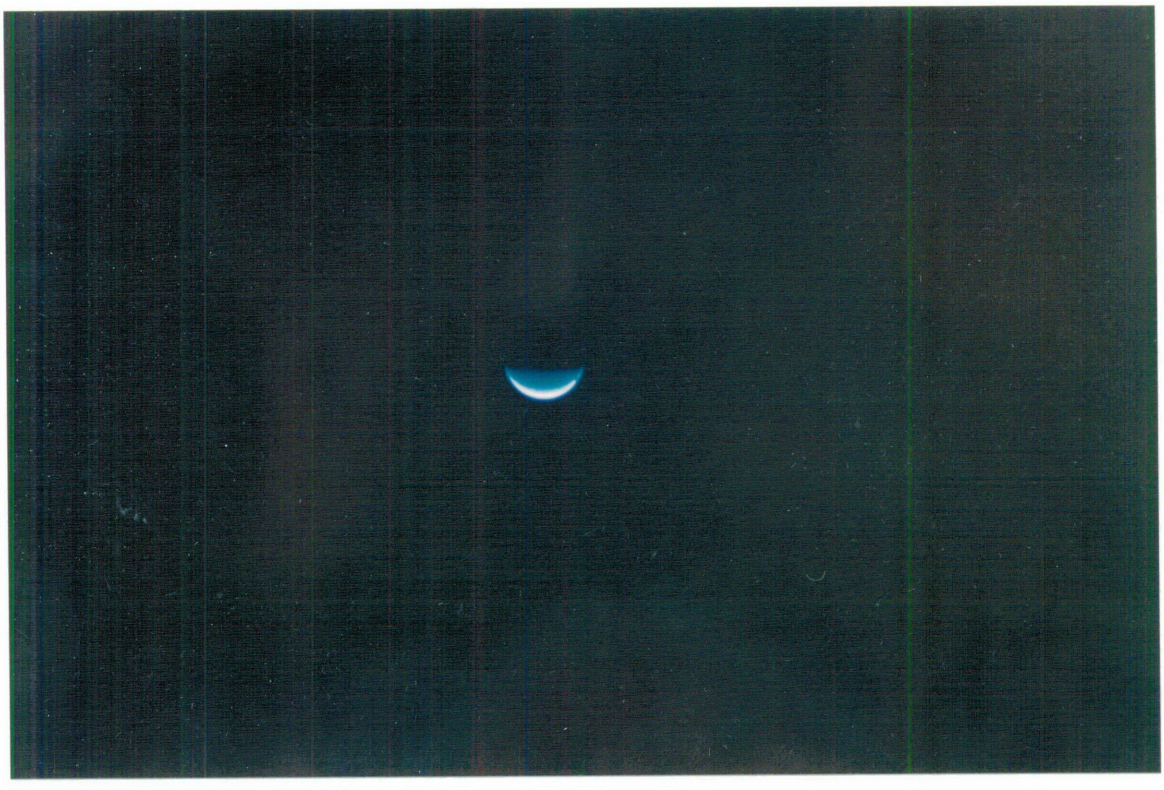

Figure 2.1 The glow produced by a self-sustained corona discharge in air.

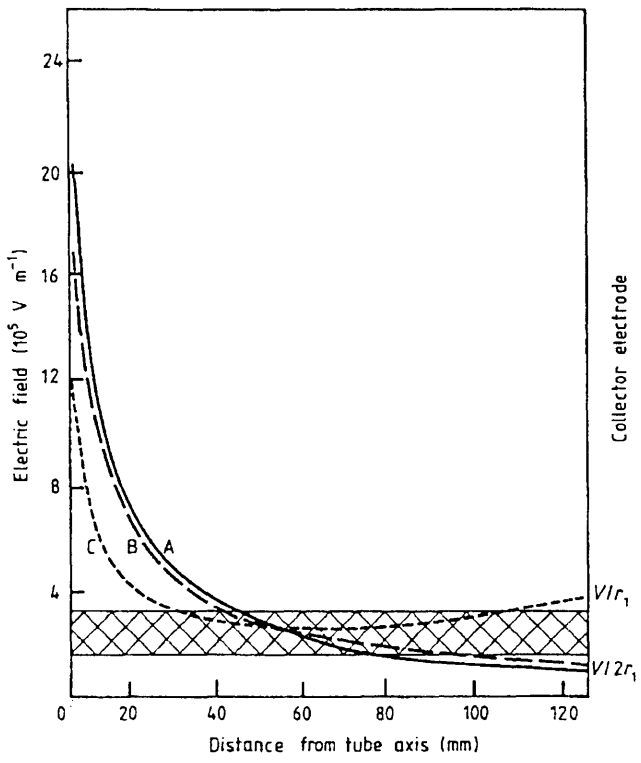

Figure 2.2 Electric field in a wire-cylinder electrode system.
A: pre-corona, B: small space charge, C: large space charge (Cross, 1987).

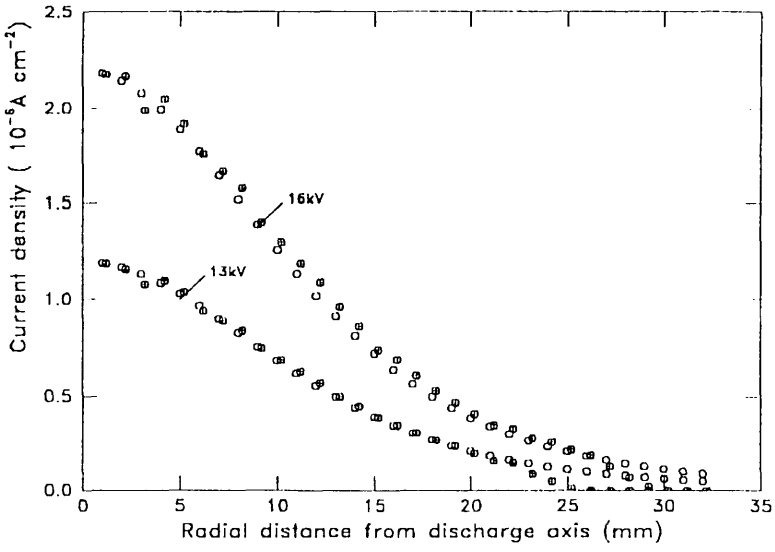

Figure 2.3 The current density on the plate of a point-plate corona discharge.
Open circles - Warburg's equation;
Crossed circles - experimental data (Lamb, 1992).

Warburg was also the first to determine an empirical current-voltage relationship for a corona discharge.

$$I = KV(V - V') \tag{2.2}$$

where V is the corona voltage, V' is the onset corona voltage and K is a geometrical constant.

In a typical open-air corona discharge with a 20 mm gap between anode and cathode, the current is of the order of tens of microamps when the point anode is raised to tens of kilovolts. Figure 2.4 shows a current-voltage relationship for a positive glow corona discharge, as obtained in the present work using the experimental arrangement detailed in Chapter 4.

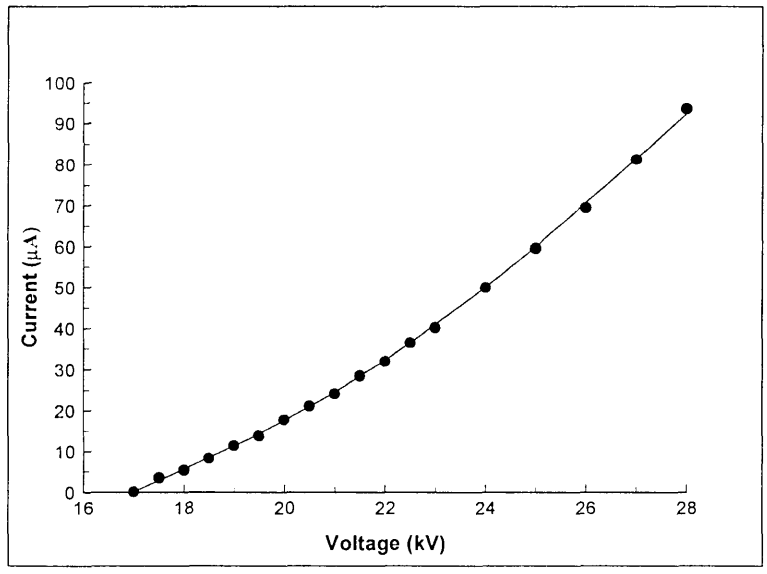

Figure 2.4 Current-voltage relationship for a positive glow corona. 15° hyperboloidal anode, discharge gap - 20 mm.

The glow is a lateral diffusion of avalanches along the point surface which causes the electric field near the point to fall and thus shields the gap from arcing (Figure 2.5-A. Sigmond, 1983). As the current is increased further, any spurious current increase at a point on the anode will increase the concentration of positive space charge in a small region close to the anode and thus weaken the field in a small volume. This weakening of the electric field results in the ionisation region being pushed out into the corona gap to act like a spiked extension of the anode (Figure 2.5-B). The change in the effective geometry of the anode causes still further avalanches to occur. Behind the head of this so-called streamer, the positive and negative charge densities are almost equal and thus constitute a weakly conducting plasma filament. This streamer process (Figure 2.5-C) is characterised by bipolar charge movement. This primary streamer may or may not extend to the cathode. If the streamer does not reach the cathode, the bipolar charges are cleared by the electric field, allowing the formation of further streamers. However, if the primary streamer bridges the discharge gap, a residual plasma channel will exist and this provides a conducting channel for secondary streamers to reach the cathode. It is the secondary streamers that lead to total breakdown of the corona gap. It is important to note that a corona discharge can operate concurrently in both the glow and streamer modes. Alternatively, a point-plane corona discharge in atmospheric air that operates as a steady glow one day, may act preferentially to give streamers the next, at the same voltage and current (Sigmond, 1983). This is because corona discharges in air are critically dependent on the moisture content of the air. The burst pulses which signal the onset of a corona discharge are also known as pre-onset streamers because their production mechanism is the same as that for breakdown streamers.

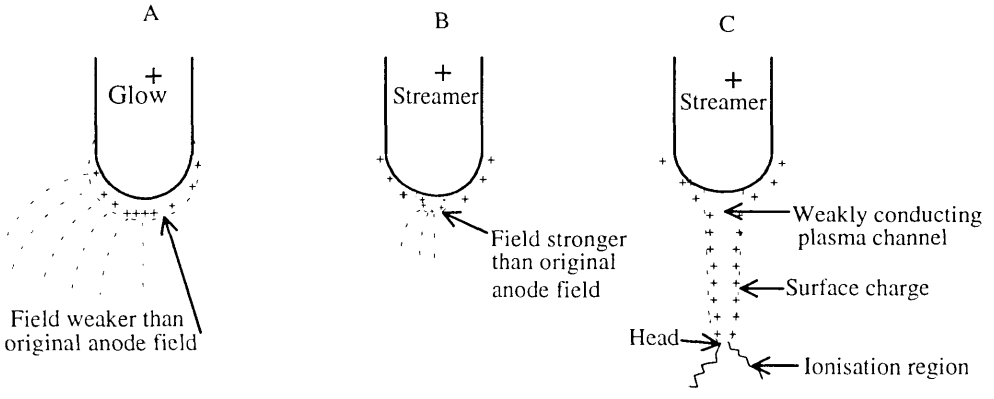

Figure 2.5 Streamer development from a stable glow corona (Sigmond, 1983).

2.1.2 The effect of pressure on corona discharges

The effect of pressure on a corona discharge comes predominantly in the form of affecting the mobility of the ions in the gas. In general, as the pressure of a gas increases, the ion mobility decreases, causing the current at a given voltage to fall. Thus, the corona onset voltage increases as the pressure increases. Similarly, the sparkover voltage of the gap increases with increasing pressure. However, there is an important exception to this: in electronegative gases or gas mixtures at high pressures the voltage does not increase fast enough to maintain a constant current without exceeding sparkover. At low pressures the sparkover voltage rises more rapidly than the corona voltage required for constant current. Hence, a graph of corona sparkover voltage as a function of pressure passes through a maximum and then falls until, at a critical value of pressure, it falls to the level of the corona inception voltage. For pressures above this, sparkover of the gap is not preceded by a corona discharge. Figure 2.6 shows the graph of the sparkover and corona onset voltages for SF_6 compared to nitrogen (N_2) which is a non-electronegative gas. These curves are for a point-to-plane electrode system with a 2.5 cm gap and an alternating voltage at 60 Hz.

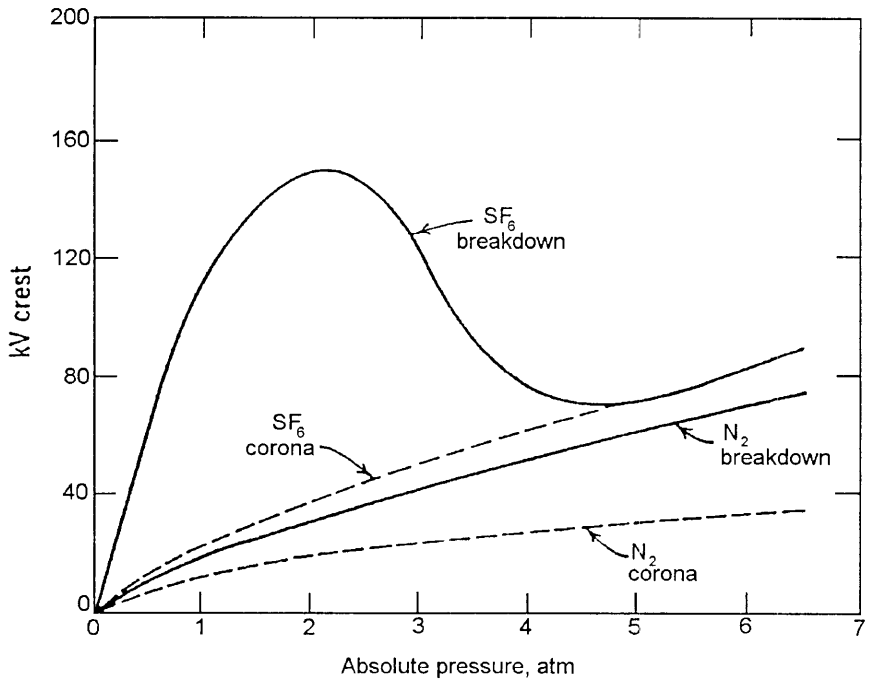

Figure 2.6 Breakdown and corona onset voltages for SF_6 and N_2 (Kirk-Othmer, 1980).

2.2 *Corona discharges in SF_6*

As stated, the characteristics of a corona discharge depend, not only on the geometry of the electrode system and the voltage on the stressed electrode, but also on the nature and pressure of the gas. Sulphur hexafluoride (SF_6) is a colourless, tasteless and odourless gas. The six fluorine atoms are grouped around and equidistant from the sulphur atom and due to this symmetric structure SF_6 is chemically inert. SF_6 has a density of 6.406 kg/m^3 at atmospheric pressure and a molecular weight of 146.1. Other SF_6 physical and thermochemical properties are listed by Schumb (1947) and Kirk-Othmer (1980). SF_6 readily forms negative ions by attachment of electrons to both the neutral SF_6 molecule and to some of its dissociation products to form such negative ions as SF_5^- and SF_6^-. Due to its electronegativity and thermal properties, SF_6 is an excellent insulator and arc-quencher and has been used for high-voltage insulation since the mid 1930s (Schumb, 1947). A more recent application of an SF_6 discharge is in the plasma etching of silicon for the fabrication of semiconductor devices (Eisele, 1981).

Corona discharges in SF_6 develop in a similar manner to corona discharges in air. However, the dielectric strength of SF_6 at atmospheric pressure is 2.35 times that of air (Deshpande, 1991). This means that the corona discharge inception voltage for SF_6 is much higher than that for air when the same electrode geometry and pressure are used. With the higher voltages there is an increased occurrence of streamer formation. Indeed, corona discharges in SF_6 are rarely seen in the steady glow mode except at low pressures (below 20 kPa) (Van Brunt and Leep, 1981). Van Brunt and Leep (1981) studied positive dc corona discharges in SF_6 at pressures from 50 to 500 kPa. They found that the positive corona discharge begins as low-level electron avalanches of low repetition rate. As the voltage increases these form into large streamers which are followed by bursts of pulses. Van Brunt and Leep found that as pressure increased in an SF_6 corona discharge the average duration of the streamer bursts decreased. They concluded that the decreasing ion mobility with increasing pressure accounted for these results. Lower ion mobility means that positive space charge will build up more rapidly and this acts to shield the discharge gap from propagating streamers. The faster the positive space charge builds up the shorter is the streamer pulse.

The mobility of positive ions (SF_5^+) has been reviewed by Brand and Jungblut (1983) and all experimental results were standardised to the reduced ion mobility b_0, at standard temperature and pressure. The reduced ion mobility is given by

$$b_0 = b\frac{P}{P_0}\frac{T_0}{T} \tag{2.3}$$

where b is the actual ion mobility, $P_0 = 760$ Torr, and $T_0 = 273.16$ K.

Figure 2.7 shows the reduced positive ion mobility for varying E/N with the dashed line being the best-fit curve to the data (Morrow, 1986). The dot-dashed line represents the value of E/N where the ionisation rate equals the attachment rate. The curve shows that the reduced ion mobility is constant for E/N < 1.2 x 10^{-15} V cm^2 and hence, as the pressure is increased the actual ion mobility does indeed decrease.

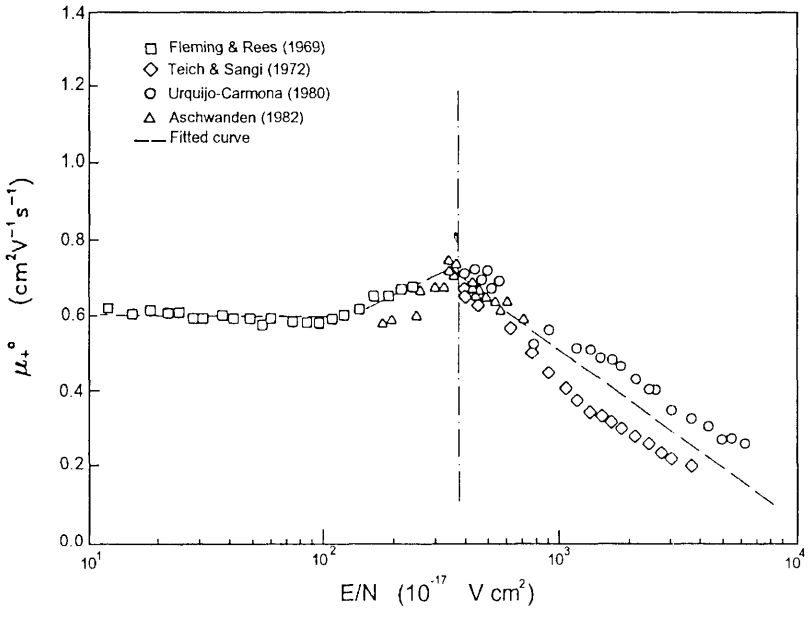

Figure 2.7 Reduced ion mobilities for positive ions in SF_6 (Morrow, 1986).

When SF_6 is used for high voltage insulation in devices such as circuit breakers (Deshpande, 1991) and electrostatic accelerators (Ophel *et al.*, 1983) the presence of a corona discharge is a problem because a current flow in SF_6 will cause dissociation of SF_6 molecules. Since the gas temperature in an SF_6 corona discharge is only a few degrees above ambient (Woolsey *et al.*, 1986), thermal dissociation of SF_6 is negligible in a corona discharge. Dissociation of SF_6 takes place via electron impact ionisation and dissociative attachment (Ogle, 1986). Some of the dissociation products of SF_6, especially fluorine, are extremely reactive. Indeed, it is this very property of SF_6 that makes SF_6 an appropriate choice of gas for plasma etching of silicon (Eisele, 1981). When impurities such as oxygen and water are present in the system the range of dissociation products is greatly increased with the oxyfluorides, SOF_2, SOF_4 and SO_2F_2 and hydrofluoric acid being among the decomposition products (Van Brunt and Leep, 1981).

The decomposition products of SF_6 are capable of attacking both non-metallic materials, such as glass and some ceramics, and metals. MacGregor *et al.* (1986) studied positive dc corona discharges in SF_6 at 200 Torr with electrodes of different materials. For electrodes made from stainless steel, brass and copper, the appearance of the corona discharge around the anode changed over time. Initially, the discharge appeared as a diffuse glow with occasional bright streamers of current up to 80 μA. After continually running the discharge for 45 minutes the corona discharge had negligible glow characteristics and was dominated by intense streamers with currents as high as 300 μA. However, when nickel was used for the anode there was little change in the appearance of the discharge over the same length of time and this is due to the fact that nickel is the least reactive of these metals with fluorine. This study highlighted how the contamination of the electrode surface, by the fluorine produced from dissociation, may affect the behaviour of the SF_6 corona discharge. There has been some discussion recently concerning the relative importance of the surface roughness and the presence of impurities in regard to the breakdown of the insulating properties of SF_6 (McAllister and Crichton, 1997; Berger and Senouci, 1997). Clearly both the state of the electrodes and the presence of impurities affect the nature of a corona discharge in SF_6 .

2.3 Applications of corona discharges

Corona discharges in SF_6 are often unwanted and can cause numerous problems. Some of these problems have been referred to in the above section and more will be discussed in relation to the corona wind in Section 2.5.3. Coronas occurring at points and sharp edges inside circuit breaker

chambers can lead to the degradation of gas and solid insulation and corrosion of conductors. Such modifications to the integrity of a circuit breaker can lead to sparking. There are also problems associated with corona discharges in air such as radio interference and corrosion of high voltage power lines. For this reason corona discharges in air and SF_6 are of considerable interest to the power industry. At the same time, corona discharges have many applications in such fields as electrostatics, plasma chemistry and, of course, gas discharge physics.

Electrostatic applications of the corona discharge rely on the fact that the discharge gap is full of ions. Coronas are used for particle charging in devices such as photocopiers, laser printers, electrocoating units and electrostatic separators used in the mining industry (Sigmond and Goldman, 1983). A particularly important corona application is the electrostatic precipitator. Precipitators are used in many industrial applications to clean exhaust gases of particulate matter prior to releasing the gases into the atmosphere. The particulate matter is charged by a corona and collected by an electric field. This process is discussed in relation to the corona wind in Section 2.5.2.

There are also applications which use the chemical reactions that occur in a corona discharge. The interactions between the flux of electrons and the gas particles lead to a transfer of energy which produces a range of chemically active species. These species can be divided into three categories; species carrying electrical charge (electrons and ions), neutral fragments of molecules (atoms and radicals), and excited molecules (Goldman and Amouroux, 1983). One important reaction which takes place in an air corona is the production of ozone. Ozone (O_3) is produced in a two-step process, involving the dissociation of the oxygen (O_2) molecule by an energetic electron and the subsequent recombination of O_2 and O (Goldman and Amouroux, 1983), according to

$$e + O_2 \rightarrow 2O + e$$

$$O + O_2 + M \rightarrow O_3 + M$$

where M may be O, O_2 or O_3.

Ozone is highly reactive and, in small quantities, can be used as a deodorising agent. Commercial units are available that use coronas to produce ozone for air purification in residential and office accommodation. However, ozone is one of the most powerful oxidants known and is toxic to humans, animals and plant life. Ozone can also cause serious deterioration in many materials. For example, in a full-scale electrostatic precipitator, both the efficiency of the particulate trapping process and the rate of ozone production is proportional to the input power (Abdel-Salam *et al.*,

1997a). This means that a full understanding of the processes involved in the corona discharge is required to enable precipitators to be designed to provide maximum trapping efficiency with minimum ozone production.

A rather unusual corona application has recently been described by Peurrung and Peurrung (1997). They have proposed an *in situ* corona discharge for the treatment of organic contaminants in soils, and performed laboratory experiments to validate this proposal. The presence of air and water in soil allows a corona discharge to be established in the soil. In this air/water corona strong oxidising agents are formed such as ozone, hydroxyl radicals and ions, and peroxide radicals and ions. These species preferentially react with contaminating organic molecules, with the result that the latter are oxidised to carbon dioxide and water.

This is, by no means, a complete list of the applications of corona discharges. However it serves to emphasise the large number of systems that utilise or are affected by coronas. The role of the corona wind in distributing chemically active species or disturbing the flow of charged particles in many of these areas needs to be considered if a complete understanding of corona discharges and corona devices is to be achieved.

2.4 The corona wind

The corona wind, sometimes called the ionic or electric wind, is a phenomenon which has been known since the early 1700s. Robinson (1962) produced an excellent review of the historical development of our understanding of the corona wind. From the first report, in 1709, by Francis Hauksbee, of feeling a weak blowing sensation when holding a charged tube near his face, to the later interest of such eminent scientists as Newton, Benjamin Franklin, Faraday, Maxwell and Becquerel, the corona wind remained something of a curiosity. The possibility of using the wind to drive an electrostatic motor was investigated but the subsequent development of the "electric fly" (an s-shaped wire suspended at its centre point, which spun about an axis when a high voltage was applied to the shaft) by Hamilton in the 1750s remained the only application of the corona wind until well into the 1900s.

Early explanations of the corona wind referred to charged particles experiencing resistance from the air, but Faraday, in 1838, pointed out that the charged air particles may well be only a small portion

of the air which is ultimately set in motion. Maxwell also held this opinion and over the years various theories of the corona wind were proposed. With the discovery of the gaseous ion by Thomson and his group at the Cavendish Laboratory of Cambridge in the late 1890s, the origin of the corona wind was confirmed (Robinson, 1962).

The present explanation for the production mechanism of the corona wind is quite straightforward. The ions produced in the high-field region near the point electrode are repelled from the point, accelerate to high speeds and collide with neutral gas molecules. These collisions result in a transfer of momentum from ions to neutral gas molecules. Molecules are thus propelled into the low-field region. As a result, there is a continuous flow of neutral gas molecules away from the point electrode, regardless of the polarity of the point. This neutral gas flow constitutes the corona wind. The movement of the neutrals causes a pressure drop around the point electrode (Loeb, 1965) and this further enhances the movement of the neutrals by drawing further gas molecules into the discharge gap from above. This pressure drop has been measured by Yabe *et al.* (1978) and is discussed in Section 2.6.1 in relation to measurement of the corona wind.

Generation of the neutral gas flow relies on ionisation near the point and it is not surprising, therefore, that the wind speed depends on both the corona current and electrode geometry. The speed of the corona wind has been found both theoretically and experimentally to be proportional to the square root of the current. For a diverse selection of electrode geometries and discharge systems, the velocity of the wind is always reported to be around a few metres per second (Thanh, 1979; Sato, 1980; Teisseyre *et al.*, 1982). It has been measured up to 0.5 m away from the discharge gap (Woolsey *et al.*, 1991). Figure 2.8 is a photograph in which the effect of the corona wind is demonstrated by seeding the corona discharge with fog particles. In the photograph the point electrode is surrounded by an insulating cylinder which aids the process of drawing the fog into the discharge gap, the grid cathode is supported by the flange visible in the top half of the photograph and the red glow within the discharge gap is due to scattering by fog particles of the laser beam associated with the laser Doppler anemometry system. The procedure of seeding the corona is described in Section 4.5.1.

Having said that the present description of the origin of the corona wind is quite simple, it is by no means a straightforward matter to develop a mathematical model describing how the production, speed and direction of the corona wind depend on the electrical discharge that produces it. Chattock (1899) was the first investigator to offer a quantitative analysis of the production mechanism of the corona wind.

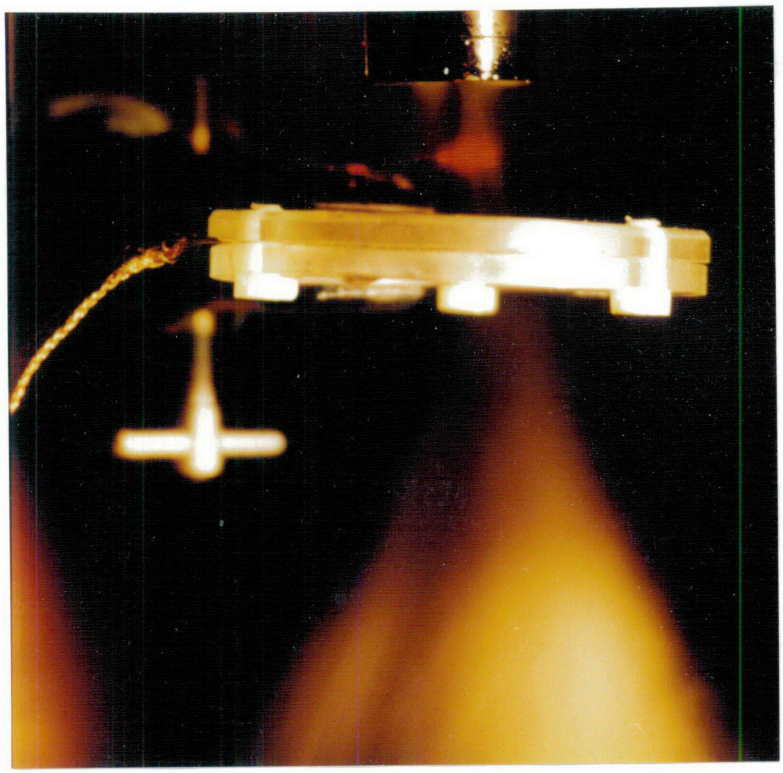

Figure 2.8 Photograph showing the effect of the corona wind.

Chattock studied a point-plane corona discharge and developed a relationship between the corona current and the pressure exerted on the plate by the movement of ions in the electric field and the corona wind, as

$$v = Iz/(P - \pi) \tag{2.4}$$

where v is the velocity of the ions in unit electrostatic field, I is the total current, z is the length of the discharge gap, P is the total fluid pressure on the plane and π is the pressure due to the movement of the neutral gas (corona wind).

Chattock noted that with a sharp point and a gas at atmospheric pressure the ions give up the greater part of their momentum very close to the point. It was not until the 1950s that Chattock's work was expanded to include other geometries and to examine the effect of the corona wind on corona discharge parameters (Kulacki, 1981). Stuetzer (1959, 1960) analysed the pressure on a plate due to the corona wind for various electrical and hydrodynamic boundary conditions using several coordinate systems. Stuetzer was primarily interested in producing a pump for the movement of liquids and it is this fluid mechanical property of the corona wind which has resulted in many of the modern applications of the wind to convective heat and mass transfer.

2.4.1 Electrohydrodynamic theory of the corona wind

A theoretical analysis of the corona wind provides many insights into the fundamental processes involved in its production and flow. The following development of an electrohydrodynamic theory of the corona wind is a combination of analyses performed by Robinson (1961, 1970), Kibler and Carter (1974), Yabe *et al.* (1978) and Kulacki (1981). The theoretical results obtained in this section are used in later chapters to examine the corona wind data obtained in the present work.

Electrohydrodynamics (EHD) refers to a coupling between either an electric field or an electrical discharge and a fluid field. The force experienced by a neutral particle within the inter-electrode space, due to the charges on the ions, is a function of location within the flow and acts throughout the full extent of the discharge gap. Thus, the fluid dynamics of the corona wind and the electric field in the corona gap are formally coupled in the corona discharge. For a full analysis of the corona wind, the effect of the temperature field on parameters such as the dielectric constant, the density of the gas and the pressure in the gas, also needs to be included. To consider all these components requires computer modelling. However, simplifications can be made throughout the development of the theory which provide a general understanding of the processes involved in the production of the corona wind to be acquired.

Figure 2.9 illustrates the interactions between the electric, fluid and temperature fields associated with the corona wind. When considering the corona wind, the major interactions are those denoted by the thick black lines in Figure 2.9.

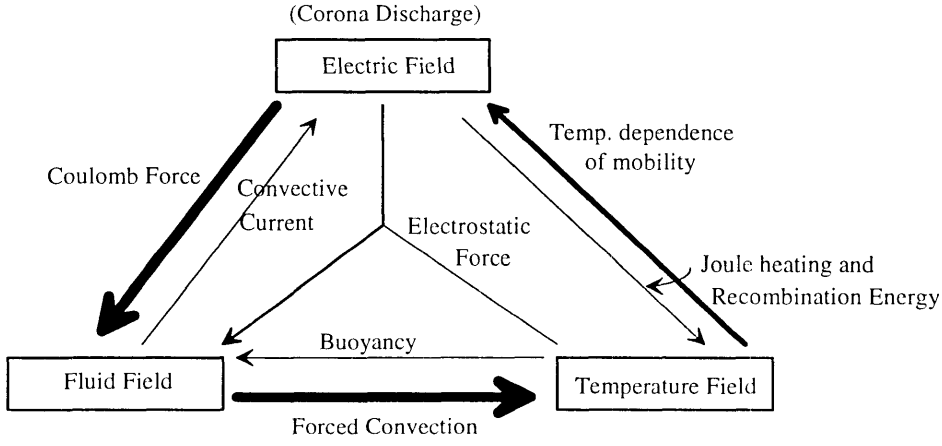

Figure 2.9 Interactions between the electric, fluid and temperature fields in a corona discharge (Yabe *et al.*, 1978).

The following nomenclature is used throughout this section:

b - ion mobility	c - specific heat of gas	$\underline{E}$ - electric field strength
$\underline{F}$ - total force on an ion	g - geometrical factor	j - current density
k - thermal conductivity	K - energy loss coefficient	p - pressure
T - temperature	$\underline{u}$ - total velocity of ion	$\underline{u}_w$ - corona wind velocity
ρ_g - gas density	ρ_c - charge density	η - gas viscosity
ε_0 - permittivity of free space	ε - dielectric constant of the gas	

For an isotropic, incompressible fluid which is free of surface forces and magnetic fields, the set of equations which needs to be considered is:

Navier-Stokes Equation
$$\underline{F} - \rho_g \underline{u} \cdot \nabla \underline{u} - \nabla p + \eta \nabla^2 \underline{u} = 0 \tag{2.5}$$

Heat transfer
$$c\rho_g \underline{u} \cdot \nabla T - k\nabla^2 T = 0 \tag{2.6}$$

Conservation of charge
$$\frac{\partial \rho_c}{\partial t} + \underline{u} \cdot \nabla \rho_c = \nabla \cdot j \tag{2.7}$$

In Equation 2.5, $\underline{F}$ is the total force on an ion and is due to a combination of the Coulomb force and the electrostatic force. The Coulomb force is the total force experienced by the ions due to their charge. Molecules in a non-uniform field will experience a force due to any natural dipole moment or will be polarised by the field and this will result in movement of the molecules toward the high field region, in this case the point electrode. This force is, therefore, in the opposite direction to the Coulomb force. Changes in the dielectric constant with temperature and density will also cause movement of the molecules and these two processes contribute to an electrostatic force. Thus,

$$\underline{F} = \rho_c \underline{E} - \frac{\varepsilon_0}{2} \underline{E}^2 \nabla \varepsilon + \frac{\varepsilon_0}{2} \nabla \left(\underline{E}^2 \frac{d\varepsilon}{d\rho_g} \rho_g \right) \tag{2.8}$$

The second and third terms in Equation 2.8 are designated as the electroconvection and the electrostriction, respectively. Except in the high-field ionising region, the electrostatic force is one order of magnitude smaller than the Coulomb force (Yabe *et al.*, 1978) because the dielectric constant and the density of the gas can be considered as uniform and independent of temperature. Hence, the effect of the temperature field as given in Equation 2.6 is negligible and only the first term on the right-hand side of Equation 2.8 remains.

$$\underline{F} = \rho_c \underline{E} \tag{2.9}$$

The third term in Equation 2.5 can be neglected if we consider that there are no changes in the fluid pressure in the stationary fluid. The fourth term in Equation 2.5 is due to any forced flow and this also can be neglected in the typical corona wind due to a corona discharge. The second term in Equation 2.5 is due to the transfer of momentum from the ions to the neutral gas molecules and is given by;

$$\frac{1}{2} K \rho_g \underline{u}_w^2 \tag{2.10}$$

where K allows for energy losses in a system which is bounded. By substituting Equation 2.9 and Equation 2.10 in Equation 2.5 we have

$$\rho_c \underline{E} - \frac{1}{2} K \rho_g \underline{u}_w^2 = 0 \tag{2.11}$$

To eliminate the electric field from Equation 2.11 the charge density in the corona gap is considered. Equation 2.7 defines the current density as the space-charge density changes over time and space. The charge density can be considered constant in a steady glow corona discharge, so that Equation 2.7 can be rewritten as

$$j = \rho_c \underline{u} \tag{2.12}$$

The velocity of the gas is a result of two simultaneous effects: the movement of charge through the main body of fluid and the transport of charge by the fluid. These two components are produced by the ion drift velocity due to the electric field and the velocity due to the corona wind. The drift velocity of the ions is given by $b\underline{E}$, where b is the ionic mobility. Thus

$$\underline{u} = b\underline{E} + \underline{u}_w \tag{2.13}$$

Equation 2.12 becomes

$$j = \rho_c (b\underline{E} + \underline{u}_w) \tag{2.14}$$

In gases, the velocity of the ionic drift in the electric field is considerably greater than the velocity due to the corona wind and the increase in the current due to the transport of charge by the fluid can be neglected. Equation 2.14 (less the corona wind component) is substituted into Equation 2.11 and rearranged so that

$$\frac{j}{b} = \frac{1}{2} K \rho_g \underline{u}_w^2 \tag{2.15}$$

To find the corona wind velocity at the plate electrode we must integrate over the cross-sectional area of the wind profile.

$$\underline{u}_w^2 = \frac{2}{K\rho_g} \int \frac{j}{b} dA \tag{2.16}$$

As the area of the corona wind changes with position through the discharge this integration is difficult. However, if we assume constant mobility and consider only the one-dimensional case of unit cross-section along the discharge axis, Equation 2.16 becomes

$$\underline{u}_w = \left[\frac{2}{K\rho_g b} \int j \, dz \right]^{\frac{1}{2}}$$

$$\underline{u}_w = g \left(\frac{I}{K\rho_g b} \right)^{\frac{1}{2}} \tag{2.17}$$

where g is an appropriate function of the electrode geometry and I is the current in the external circuit. Thus, the velocity of the corona wind is proportional to the square root of the corona current. Since the corona current is proportional to the square of the corona voltage it follows that the velocity of the corona wind is directly proportional to the corona voltage.

In the above theory, many assumptions have been made and many terms neglected in order to handle the mathematics. A more precise description of the corona wind, in terms of discharge parameters, requires computer analysis.

Yabe *et al.* (1978) conducted experiments using a single platinum wire discharging above a copper plate electrode, with nitrogen as the working fluid. They used a Langmuir probe to measure the electric field generated by their corona discharge and a manometer to measure the static pressure on the plate electrode. Their experimental results of the potential distribution along the axis of the discharge gap are shown in Figure 2.10 and show the change in the electric field as a result of the presence of space charge. It can be seen that the space charge modifies the potential distribution in

the gap and this underscores the need for a solution of the completely coupled, electrical and fluid, problem.

Yabe *et al.* went on to perform a theoretical analysis of their problem but decoupled the electric and fluid fields by introducing the following assumptions:

- since the spatial and density variations of the dielectric constant ε in air are usually small in the discharge region, except in the very narrow high-field ionisation region around the point, the electrostatic force can be neglected;
- there are only neutrals and ions of one sign in the field;
- the diffusion of ions is neglected, as its effect is much less than the effect of drift due to the electric field;
- the drift velocity of the ions is given by bE.

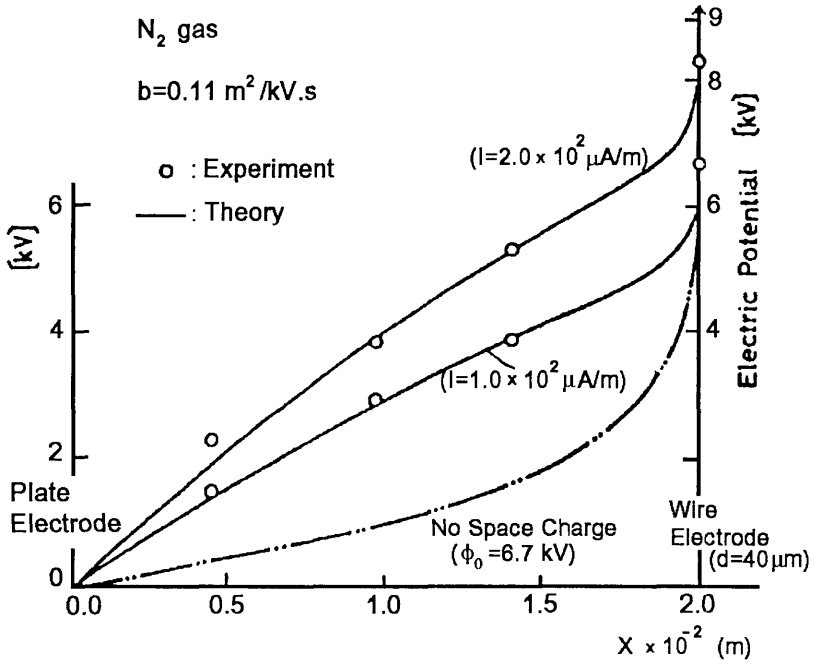

Figure 2.10 Electric potential distribution along the axis of the discharge (Yabe *et al.*, 1978).

Yabe *et al.* solved the electric field problem first and then the calculated Coulomb force was used to analyse the fluid field. The results of the electric field and fluid field analyses are presented in Figures 2.11 and 2.12 respectively, along with some of their experimental data. The calculated space potentials within the discharge gap are very close to that measured with the Langmuir probe. Figure 2.12 shows the recirculation of the fluid flow caused by interaction with the plate electrode and boundary walls.

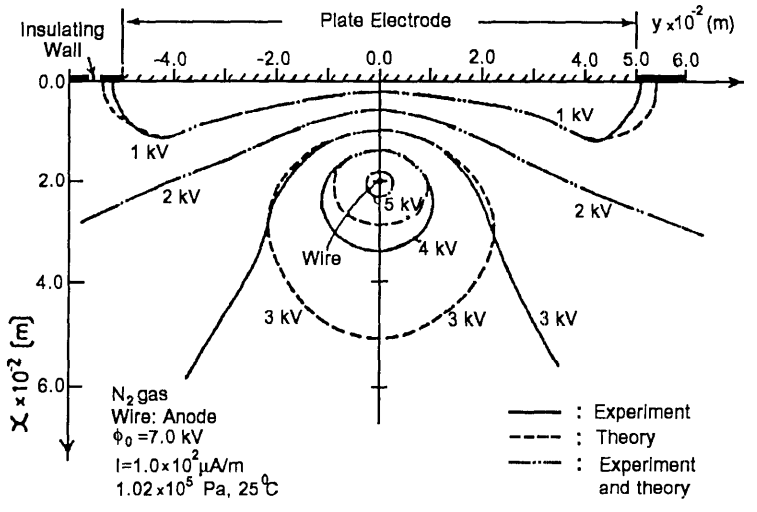

Figure 2.11 Measured and calculated space potential distribution (Yabe *et al.*, 1978).

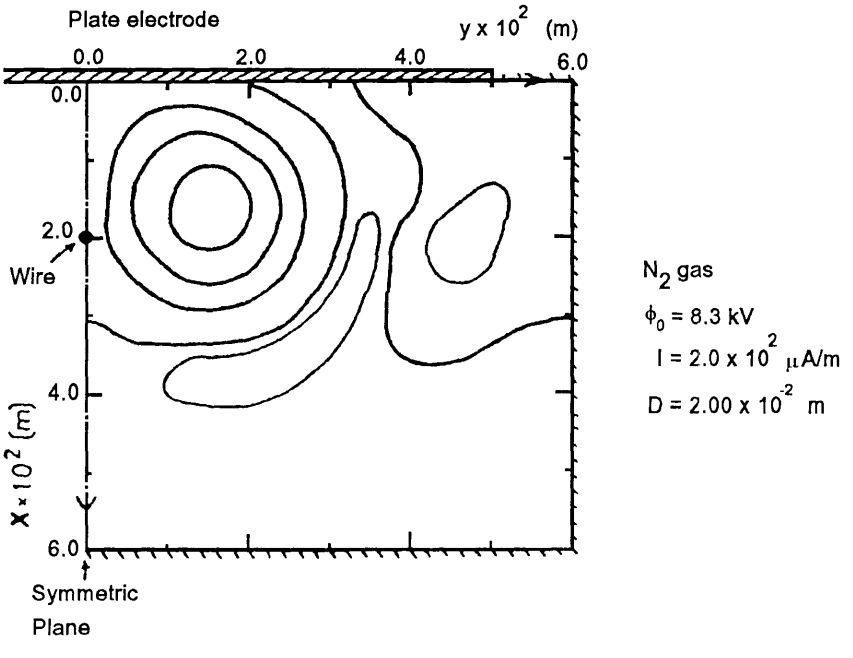

Figure 2.12 Circulating corona wind flow (Yabe *et al.*, 1978).

2.4.2 The effect of pressure on the corona wind

Equation 2.17, which relates the corona wind speed $\underline{u}_w$, to the corona current I, involves the product of the gas density ρ_g, and the ionic mobility b. For a given gas the product $\rho_g b$ is approximately constant and independent of density, ambient pressure and temperature. It follows that the speed of the corona wind should also be independent of the parameter $\rho_g b$. Robinson (1961) used a point-screen electrode configuration and found the velocity of the corona wind below the screen as a function of the density of the air. The results of this experiment are reproduced in Figure 2.13. It can be seen that for gas densities greater than one atmosphere the corona wind speed can be considered constant at any one current and position. Below one atmosphere in pressure the curves begin to decline. As Robinson has not included data points at very low pressures it is difficult to determine the exact shapes of the curves at low pressure. To determine the effect of low pressure on the corona wind the product $\rho_g b$ should be considered for the gas in question. Indeed, to compare the corona wind speed in systems of differing pressure and gases, such as air and SF_6, this process is a necessity. The dotted line which constitutes a boundary to the curves is the sparkover voltage at each pressure, which was discussed in Section 2.1.2.

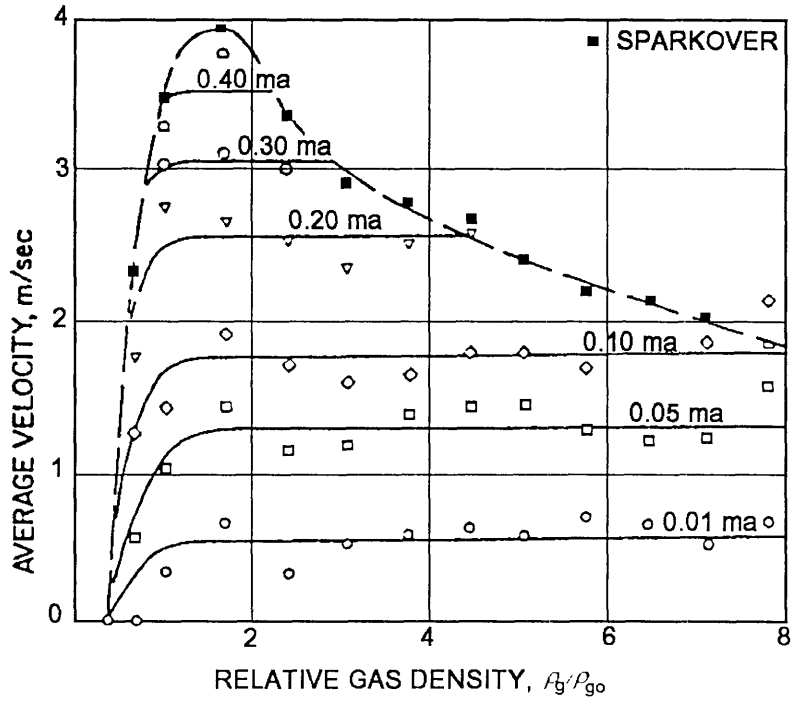

Figure 2.13 Corona wind velocity at different pressures (Robinson, 1961).

2.5 The corona wind in practical systems

2.5.1 Heat-transfer applications

The corona wind has excited interest as a means of providing localised heat transfer. It has been shown to be useful for distributing heat evenly in ovens for commercial bread baking (Kulacki and Daumenmier, 1978; Curry, 1987), enhancing mass transfer (Chen and Barthakur, 1991), cooling surfaces (Bradley and Hoburg, 1985; Yabe and Maki, 1988); and putting out fires in flammable liquids (Sher *et al.*, 1993).

Early work on the heat transfer from an object due to the presence of an inhomogeneous electric field produced a number of theories to explain this heat transfer. Kibler and Carter (1974) review some of the mechanisms which early workers used to explain cooling of an object due to the presence of a corona. These include an electrostrictive effect due to non-uniform electric fields, an electrically induced increase in the thermal conductivity of the gas, and some unknown process affecting the bulk cooling of the solid.

As detailed in Section 2.4.1, the corona wind speed can be shown theoretically to be proportional to the square root of the corona current. The forced convection heat-transfer coefficient for a circular plate exposed to a wind similar to the corona wind is proportional to the square root of the wind velocity. Kibler and Carter (1974) have provided a theoretical expression for the forced convection heat-transfer coefficient due to the corona wind; namely,

$$h_c \cong \left(\frac{2k_f}{D(\pi v)^{\frac{1}{2}}} \right) \left(\frac{2sI}{\mu\rho} \right)^{\frac{1}{4}} \tag{2.18}$$

where k_f is the thermal conductivity of the surface film, v is the kinematic viscosity, D is the plate diameter, s is the discharge gap, I is the corona current, μ is the ionic mobility and ρ is the electric charge density.

Thus the forced convection heat-transfer coefficient h_c is a function of the surface to be cooled (its diameter and thermal conductivity), the fluid properties of the gas (viscosity and ionic mobility) and the electric discharge (corona current and charge density). Kibler and Carter showed, by using a point-plane electrode system with the ground electrode heated, that the convective heat-transfer

coefficient varies according to the fourth root of the corona current as predicted by Equation 2.18. This indicates that electrocooling involves convective cooling by the corona wind.

There have been numerous studies into heat transfer using various electrode geometries, (Konno *et al.*, 1983; Franke and Hutson, 1984; Yabe *et al.*, 1987 and Kohya *et al.*, 1987), and all attribute heat transfer enhancement by a corona to convective cooling by the corona wind. Velkoff and Godfrey (1979) further investigated heat transfer by the corona wind by including external air flows which were perpendicular to the direction of the corona wind. Enhanced heat transfer was seen with air flow speeds up to the order of the corona wind speed but decreased with higher air flow speeds. Bradley and Hoburg (1985) looked at the heat transfer enhancement due to the injection of an ion flux by attempting to block the corona wind. This was done by placing a fine mesh in the discharge gap to arrest the corona wind but allow the ion flux to pass through. Results from this experiment suggested that heat transfer enhancement did take place but was not as great as when the corona wind was present. Since the experiment incorporated no method to determine if the corona wind had been completely blocked and an ion flux was maintained, these results need to be treated with care.

The amount of heat transferred from a body placed in a corona depends on the applied voltage, the shape, number and location of the electrodes and the type of electric field (negative, positive, ac or dc corona discharge). Each of these parameters exerts some degree of control over the speed and direction of the corona wind. Asakawa (1976) found that a corona could increase the rate of heat transfer in a gas by up to 1.5 times, in liquids by up to 2.0 times and in solids by up to 1.6 times.

Not only does the presence of the corona wind increase heat-transfer rates but it also enhances mass transfer. Asakawa (1976) showed that a corona generated above a water surface increases the evaporation rate by 40 to 50 times. This process has recently been used by Chen and Barthakur (1991) in a corona study which examines mass transfer enhancement in techniques for drying food, soil and agricultural products.

Sher *et al.* (1993) used a corona discharge over a small pool of isopropanol to extinguish a fire in the isopropanol. Although the electromechanical efficiency of the method was extremely low, Sher *et al.* suggested that directing the corona wind at a pool fire in a corrosive or hot environment could have advantages over more conventional fire-extinguishing techniques.

From the above discussion it is clear that the corona wind is particularly applicable to areas where small, directed jets of gas are required. In order to further develop the technological application of

the corona wind, information is required on the exact profile of the corona wind and the fundamental processes involved in its production.

2.5.2 Electrostatic precipitation

Fly-ash and dust from exhaust gases in coal-burning power stations must be collected before they enter the atmosphere. An average size boiler will produce around 25 tonnes per hour of fly-ash (Paulson, 1991). Dust collection efficiencies must be very high, around 99.5%, as council restriction on the maximum outlet dust loading can be as low as 0.1 g/m^3 from an inlet loading of 20 g/m^3 (Paulson, 1991). The electrostatic precipitator, which uses a corona discharge to charge particles and separate them from the gas flow, was invented by Cottrell in 1907 (Zhibin and Guoquan, 1994) and now is used extensively in many industrial processes for the cleaning of exhaust gases. An electrostatic precipitator must provide three basic functions:

- charging of the particulate matter;
- collection of the particulate matter by a grounded electrode;
- removal of the collected material from the electrode.

These operations are usually performed by flowing the exhaust gases from the power generation process past a wire and an earthed electrode. By applying a high dc voltage to the wire, a corona discharge is formed and the ions produced in the high-field region attach themselves to the dust and ash particles. These charged particles then drift along the electric field and are collected by the earthed electrode. The layers of collected particles are removed from the collecting electrode by periodically vibrating the electrode so that the neutralised particles fall and are collected in bins. Figure 2.14 shows the usual geometry of a duct-type precipitator.

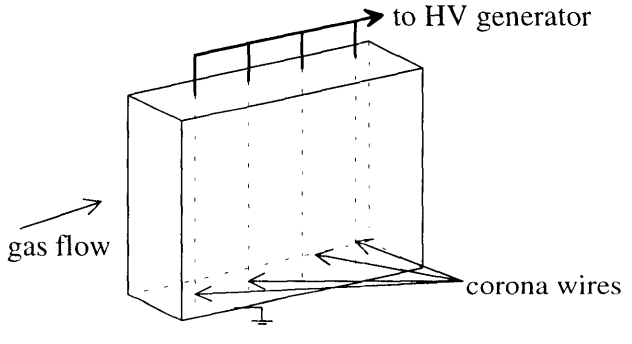

Figure 2.14 Geometry of a duct-type precipitator.

The conventional theory used for the efficiency of the precipitator is based on the Deutsch equation,

$$\log_{10}(1 - \varepsilon_p) = \log_{10}(1 - \varepsilon_m) - \alpha w_{es} / 2.303 \qquad (2.19)$$

where ε_p is the fractional efficiency of the precipitator, ε_m is the precipitator efficiency with no electric field, w_{es} is the component of mean particle drift velocity due to the movement of charged particles in an electric field and α is the specific collecting area (Paulson, 1991).

This model has long been used to estimate the collection efficiency in a precipitator. However, it neglects such factors as entrainment of particles back into the gas flow and turbulent diffusion. Work by such researchers as Cooperman (1981) and Leonard *et al.* (1983) has presented mathematical models to examine the problem of particle transport in precipitators and Zhibin and Guoquan (1994) have considered the collection efficiency of a precipitator with turbulent effects. The influence of the corona wind on precipitator efficiency was neglected by Deutsch. Larsen and Sørensen (1984) modelled the effect of the corona wind on the collection efficiency and found that turbulence caused by the corona wind decreases the efficiency of the precipitator. Davidson and Shaughnessy (1986) measured gas velocities 46 cm downstream of the corona wires using a hot-film anemometer. As expected, evidence of turbulence and secondary flows was found and they attributed this to the effect of the corona wind. Work has been done to visualise the gas flow in precipitators and to model the effect of the corona wind on the collection parameters (Kallio and Stock 1990; Davidson and McKinney, 1991; Riehle and Löffler, 1992). All this has added to our knowledge of the electrostatic precipitation mechanism but the problem remains that taking measurements of the gas flow within a working precipitator is difficult because of the presence of high voltages. In an extension of the present work, it has been possible to demonstrate the use of an optical fibre Fizeau interferometer as a probe to measure the corona wind in a working precipitator (Scelsi *et al.*, 1996). Due to its insulating nature this device allowed measurements to be made within a few millimetres of the 45 kV corona wires.

At present, the role of the corona wind in the electrostatic precipitation process is not fully understood, yet all evidence points to it detracting from the efficiency of the process. It appears that the corona wind generates turbulence which reduces the trapping rate of charged particles.

2.5.3 High-voltage gas insulation

SF_6 is now widely used in high voltage electrical equipment as an insulating medium. Section 2.2 has described the use of SF_6 in high-voltage switchgear. SF_6 is also used to insulate underground transmission lines and high voltage electrostatic generators.

As noted in Section 2.2, corona discharges and arcs in SF_6 cause the SF_6 to dissociate, with the accompanying production of corrosive by-products. Ophel *et al.* (1983) describe the use of corona discharges in SF_6 to establish a uniform electric field gradient between the high voltage terminal and ground in an electrostatic accelerator. The accelerators are run with high continuous power levels and coronas occur at many points along the length of the accelerator. The dissociation of the SF_6 under these conditions requires continual maintenance of the system. The need for monitoring SF_6 high voltage insulation is critical if performance of the devices is to be maintained. Much work has been done on the problem of monitoring gas insulation systems, especially where the system is closed, as in switchgear. The Fourth International Conference on Properties and Applications of Dielectric Materials (1994) contained numerous papers on techniques to test for the presence of corona discharges within gas and solid-insulated systems. Many monitoring systems look for the presence of corona discharges by testing for voltage pulses on the lines (Moorthy *et al.*, 1994), light from the discharge (Casanovas *et al.*, 1991), acoustic emissions (Mukai *et al.*, 1994) and radio transmission interference (Li Yao and Qi Su, 1994). The present methods of corona discharge monitoring suffer from the fact that there is substantial electromagnetic interference in the area of testing from other parts of the system. The main sources of interference are coronas on transmission lines or other nearby equipment, high frequency signals from protection units within the power system, radio broadcasts and operation of switching mechanisms in the circuit (Wang Changchang *et al.*, 1994).

The action of the corona wind within the SF_6 insulating system will affect the recombination of SF_6 dissociation products to reform into SF_6 and the settling out of the solid by-products within the device. Perhaps testing for the presence of the corona wind in a gas insulated system could be used as an approach to monitoring. Up to the present, it appears that no report on research into the corona wind in SF_6 has been published.

2.6 *Measurement of the corona wind speed*

The corona wind can be studied by traditional methods used for fluid flow visualisation. For example, Figure 2.8 was obtained by making use of the pressure drop around the anode, due to movement of the neutrals, to draw fog particles into the corona wind. Leonard *et al.* (1983) used Schlieren visualisation, along with other techniques, to study turbulence in an electrostatic precipitator and Kallio and Stock (1990) used smoke as the flow tracer in their study of the effect of the corona wind on the flow of gas through a wire-plate electrostatic precipitator. Whilst these methods confirm the jet-like appearance of the corona wind, the direction of the flow and the interaction of the corona wind with other gas flows, they provide little information on the speed of the corona wind.

Measurement of any parameter within a corona discharge is very difficult, as physical probes within the discharge gap disrupt the electric field or are themselves affected by the discharge. Thanh (1979) used a thermistor, which was placed in a corona gap, to measure the corona wind speed. However, the ions impinging on the thermistor so disrupted the measurement that a grid electrode had to be introduced to collect the ions. Consequently, corona wind speed measurements using this method could be made only below the grid.

In general, measurement of the corona wind speed with physical probes has been confined to regions outside the discharge gap, while measurements made within the gap have been made using optical techniques. The various approaches to corona wind speed measurement are now reviewed.

2.6.1 *Pressure measurement with manometer systems*

When Chattock (1899) developed the first quantitative analysis of the corona wind, (see Section 2.4), the velocity of the corona wind impinging on the plate electrode was related to the total fluid pressure on the plate. At that time, he used an opening in the plate electrode and a moving point electrode to measure the pressure change across the surface of the plate. The opening was connected, via a tube, to a U-tube water-pressure gauge. His results are of considerable historic significance and are presented in Figure 2.15. Chattock measured the pressure on the plate for both a negative corona (dashed curves) and a positive corona (full curves). Curves *a* and *c* were obtained for point-plane geometry with corona gaps of 1.91 cm and 0.2 cm, respectively. The curves marked

b were obtained by placing a disc around the point electrode. This disc was included to change the shape of the electric field in the gap to more closely represent that in a parallel plane electrode configuration. The corona gap in this case was similar to that for curve *a*. From these results Chattock concluded that the pressure measured at the plate was due to transfer of momentum from the ions to the neutral gas by friction as the ions were dragged through the gap by the applied electric field.

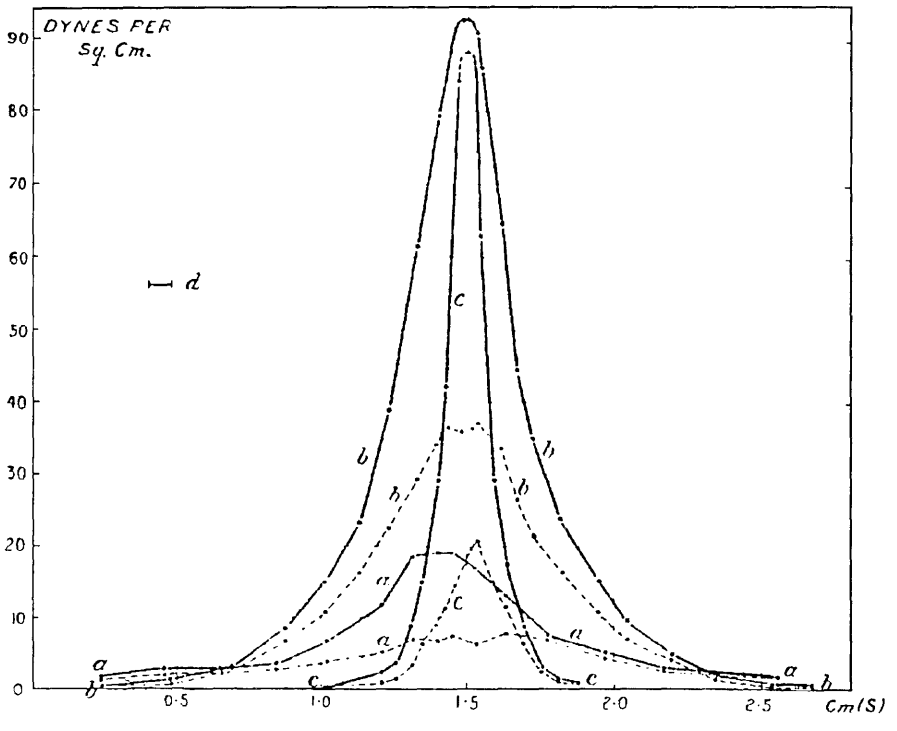

Figure 2.15 The pressure on a plate electrode due to the corona wind.
Curves *a* and *c* are for point-plate electrodes.
Curves *b* have a surface around the point electrode to simulate parallel plates.
Dashed curves - negative corona discharge; Full curves - positive corona discharge (Chattock, 1899).

A Pitot tube is an instrument for measuring the speed of a fluid and consists of a tube with two openings. One opening faces the flow and one does not. The pressure difference between the two openings provides a measure of the speed of fluid flow. Allen *et al.* (1980) and Sher *et al.* (1993) used Pitot tubes to measure the corona wind speed at various positions outside the discharge gap and on the plane of the plate electrode. Speeds of 1 to 2 m/s were reported.

Yabe *et al.* (1978), in their study of a corona discharge in nitrogen, measured the pressure at the centre of the plate electrode in a wire-plate corona discharge with a 'Chattock' gauge, which appears to be the measurement technique used by Chattock (1899). To measure the pressure around the wire a fine tube was substituted and used as the electrode. The tube had openings along its length which faced the plate electrode. Using this device, Yabe *et al.* found that the pressure around the tube had decreased by 7 Pa for a current of 110 μA and by 13 Pa for a current of 220 μA, below the static pressure in the vessel. Yabe *et al.* equated the 7 Pa pressure drop with a flow velocity of about 3 m/s.

Although Pitot tubes and other manometer techniques are useful, they do not allow measurement of the corona wind speed within the discharge gap.

2.6.2 Anemometry

An anemometer is an instrument used to measure the speed of a wind or gas flow (*anemo* - prefix meaning wind). Hot-wire, hot-film and laser Doppler anemometers are all established flow-measuring devices and each has been employed in the measurement of the speed of the corona wind.

Hot-wire anemometers and hot-film anemometers require a wire or film to be heated by a fixed flow of current (the constant-current anemometer) or to be maintained at a constant temperature by adjusting the current flow (the constant-temperature anemometer). The flow of a fluid across the wire or film causes a change in the resistance of the wire or film due to convective cooling and thus the fluid velocity can be measured. These types of anemometer have been used to study the speed of the corona wind by several researchers (Thanh, 1979; Davidson and Shaughnessy, 1986; Chen and Barthakur, 1991). These anemometers have the advantage of very small dimensions with wire diameter < 10 μm and thin film < 0.1 μm thick on a 50 μm thick ceramic base (Roberson and Crowe, 1993) but have the disadvantage of being electrically active. With this technique wind speeds of a few metres per second are reported but distortion of the electric field could well affect

the measurements. The optical fibre sensor used in this work, and detailed in Chapter 3, also uses this convective-cooling principle but has the advantage of being made from a dielectric material.

2.6.3 Laser Doppler anemometry

Laser Doppler anemometry (LDA) is another conventional flow measurement technique and there are many books on the topic, such as Drain (1980) and Durst *et al.* (1981). LDA was first proposed in the 1960s and some of the early work on this subject was by Yeh and Cummins (1964) and Foreman Jr. *et al.* (1965). LDA relies on measurement of the Doppler shift in the Rayleigh scattered light from particles moving with the flow velocity. There are two main types of LDA; the reference beam technique and the differential Doppler technique. Choice of technique depends on the properties and accessibility of the flow to be examined. In this thesis, results are presented which have been obtained by the differential Doppler technique.

A diagram of a typical differential laser Doppler (LD) anemometer is shown in Figure 2.16. Two parallel light beams of equal intensity are focussed to a point, called the probe volume. The light beams cross and produce an interference pattern of alternate light and dark fringes. Any particle moving through the probe volume will scatter the laser light. This scattered light is frequency-shifted due to the Doppler effect and is focussed on a photodetector. Since the flow directions relative to the two laser beams are different, the frequencies of the light scattered from the two beams are slightly different.

A beat frequency f_0 results from this frequency difference. The beat frequency is proportional to the particle speed and, for the configuration of Figure 2.16, is given by

$$f_0 = \frac{2v}{\lambda} \sin\frac{\alpha}{2} \tag{2.20}$$

where v is the velocity of the particles, λ is the wavelength of the light and α is the angle between the beams. The development of this relationship is given in Appendix B.

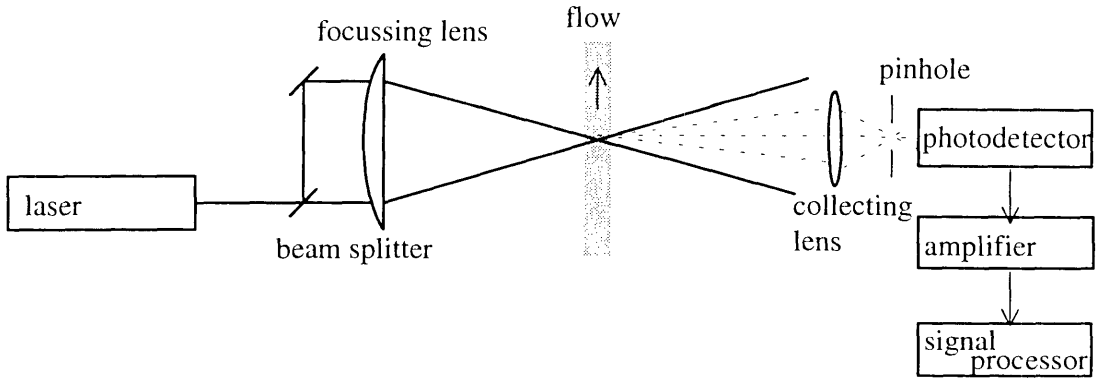

Figure 2.16 Optical arrangement for a differential laser Doppler anemometer (Drain, 1980).

The operation of the LD anemometer relies on the presence of particles to scatter the light. These particles need to be small enough to move with the flow velocity. In liquid flows, impurities usually provide the necessary scatterers. However, unless dust particles are present, gas flows need to be seeded. An article by Melling and Whitelaw (1973) details the criteria which limit the choice of particle type and the means of generating the particles. They found that the choice of scattering particle depends on the fluid temperature, the rate of fluid flow and the signal-processing system. However, in general, the scattering particles need to be of the order of 1 to 5 μm in diameter to scatter light of visible wavelengths and, for corona discharge studies, they should not be metallic.

LDA appears to be an ideal technique with which to probe the corona wind as no physical probe needs to be introduced into the corona gap. The problem with LDA is that particles introduced into the corona discharge become charged by the ions in the discharge gap and then move under the influence of the electric field. This is exactly the process which is utilised in electrostatic precipitators and other corona charging devices. The charged particles are thus moving under the combined influence of electrostatic processes and the corona wind. Hence, LDA overestimates the speed of the corona wind.

Despite this draw-back, LDA has proved to be a non-intrusive technique to study flows in harsh environments and has been utilised by researchers such as Sato (1980), Teisseyre *et al.* (1982) Leonard *et al.* (1983) and Mityushin *et al.* (1984) to study the speed of the corona wind. Sato (1980) was interested in the speed of the charged particles in a corona discharge, not the corona wind.

However, he recognised the fact that the speed of the particles is affected by the both the corona wind and the charge on the particles. Sato used LDA to measure the speed of the particles in a point-mesh corona discharge and measured the speed of the corona wind beneath the mesh by a Pitot tube. Sato's results are shown in Figure 2.17 and it can be seen that the component of particle speed due to the corona wind is the larger component.

Teisseyre *et al.* (1982) used LDA to measure the speed of dust particles in atmospheric air and Leonard *et al.* (1983) used it to measure the speed of particles in a wire-plate electrostatic precipitator. Both groups found that the corona wind had a speed of the order of a few metres per second. Mityushin *et al.* (1984) used a reference beam LD anemometer to study the corona wind in a point-plane corona discharge but provide little other information about their experimental procedure. No mention is made of the relative contributions to the speed from the corona wind and the electric field. Their three-dimensional results are presented in Figure 2.18 and are assumed to include the electric field contribution to the speed.

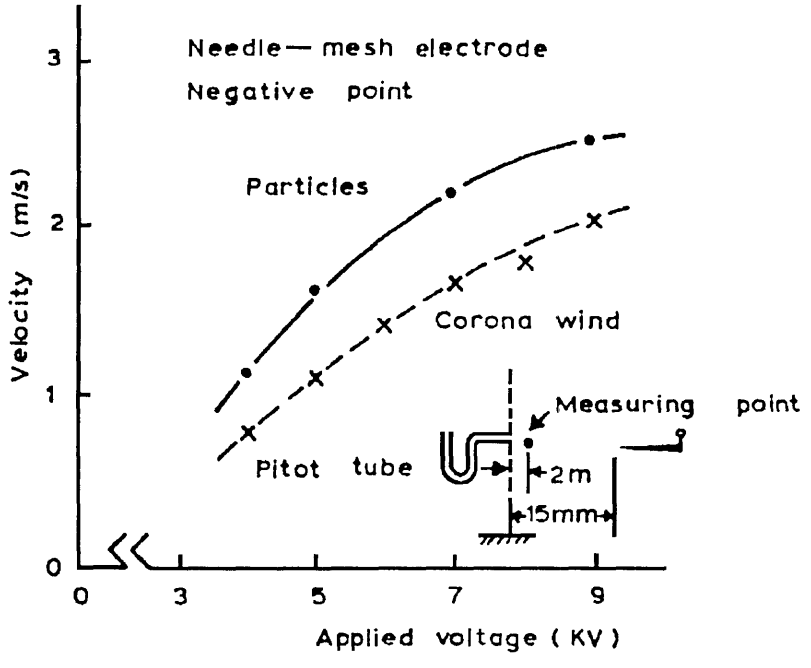

Figure 2.17 The speed of the charged particles in a corona discharge obtained by LDA compared to the speed of the corona wind (Sato, 1980).

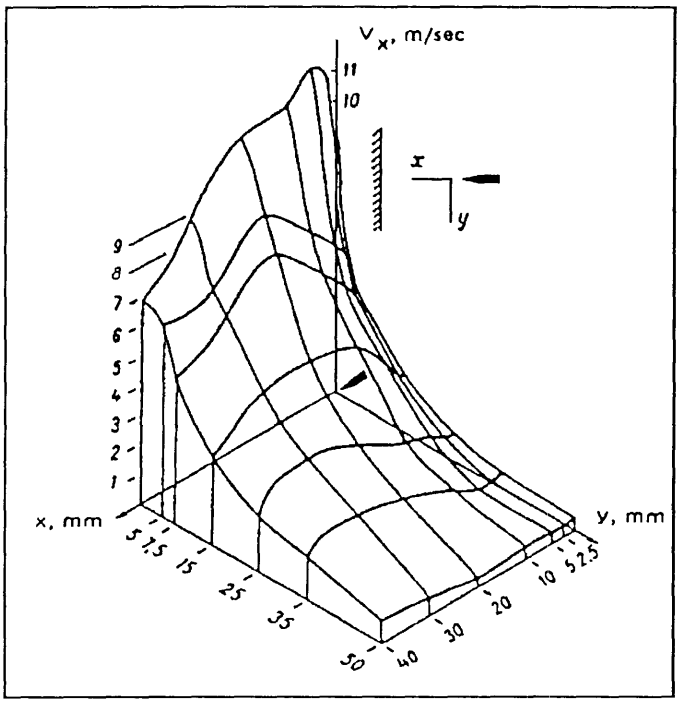

Figure 2.18 Corona wind speed profile obtained by LDA (Mityushin, 1984).

In order to avoid disturbances to the discharge, optical techniques can be employed. Tajalli *et al.* (1989) used a Schlieren technique to measure the speed of the corona wind in streamers. This technique uses the fact that the region of high speed flow has a different density and refractive index from the bulk of the fluid. The technique can be used only on the discharge axis and within a region along successive streamer paths. It is unsuitable for use in a glow corona discharge because large enough density gradients are not produced. Figure 2.19 shows the results obtained by Tajalli e*t al.* together with some wind speeds obtained by Woolsey *et al.* (1991) using laser Doppler anemometry. Included in the results are some points obtained by Lamb (1992) using a 'hot-fibre' anemometer to measure the corona wind speed at one position in a corona discharge. The details of this anemometer are presented in Chapter 3, along with improvements which led to the development of one of the wind measurement techniques which has been used in the present study.

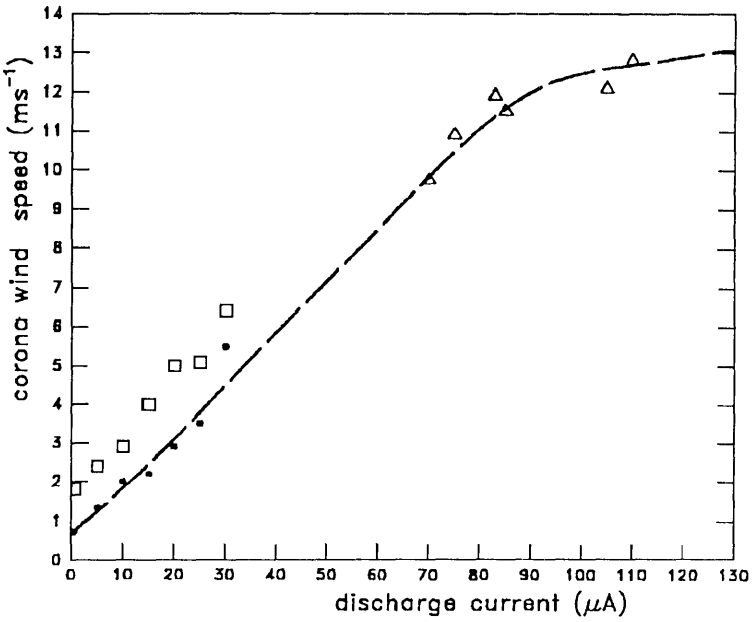

Figure 2.19 Corona wind speed in a point-plane discharge obtained by various optical techniques (Lamb, 1992).

□ LDA (Woolsey *et al.*, 1991);

• 'Hot-fibre' anemometer (Lamb, 1992);

Δ Schlieren measurements of corona wind speed in positive corona streamers (Tajalli *et al.*, 1989).